

Measurement of Finger Posture and Three-Axis Fingertip Touch Force Using Fingernail Sensors

Stephen A. Mascaro, *Associate Member, IEEE* and H. Harry Asada, *Member, IEEE*

Abstract—When the human fingertip is pressed against a surface or bent, the hemodynamic state of the fingertip is altered due to mechanical interactions between the fingernail and bone. Normal force, shear force, and finger extension/flexion all result in different patterns of blood volume beneath the fingernail. This phenomenon has been exploited in order to detect finger forces and finger posture by creating a photoplethysmograph “fingernail sensor,” which measures the two-dimensional pattern of blood volume beneath the fingernail. In this paper, a filter is designed to predict the normal force, lateral shear force, longitudinal shear force, and bending angle based on readings from the fingernail sensor. Linear, polynomial and neural network models relating the bending angle and touch forces to optical sensor outputs are developed and tested. A method is developed to uniformly calibrate the predictor for each user. Calibration experiments are performed to train and validate the predictor for seven human subjects. Results show that on average, shear forces can be predicted with 0.5 N RMS error, normal force with 1 N RMS error, and posture angle with 10 degrees RMS error. Applications and methods for improving performance are discussed.

Index Terms—fingernail, finger bending, haptic, photoplethysmograph, shear force

I. INTRODUCTION

MEASUREMENT of fingertip forces and posture plays an increasing role in the fields of robotics, haptics, and virtual reality [1]–[2]. Fingertip forces are critically important for understanding human manipulation and grasping [3]–[5]. Several researchers have investigated the force response of the human fingerpad [6]–[9]. In addition to a better understanding of human manipulation and grasping, resulting analyses lead to better characterizations of the human haptic sense, ergonomic design criteria [6], and performance criteria for haptic feedback devices [10].

Measurement of fingertip forces is also useful for acquiring skills to train robots [11], monitoring human behavior [12], and understanding human intentions for teleoperation of

robots and human-machine interaction [13]–[15]. In addition to normal touching forces, shear forces, or sliding forces in the plane of the contacting surface, play an important role in human sensing and manipulation of objects [16]–[18].

Forces acting at the fingertip are usually measured by placing force-sensing pads beneath the fingerpad, blocking off the human’s natural haptic sense. Likewise, finger posture is usually measured by wearing electronic gloves, which cover the finger and interfere with natural bending motion. Recently a new type of sensor has been designed by the authors to measure fingertip forces and posture without covering the fingertip. This photoplethysmograph fingernail sensor optically measures the pattern of blood volume beneath the fingernail, which changes when force is applied to the fingertip. This pattern can then be used to predict the fingerpad forces. Normal forces, shear forces, and even changes in finger posture have all been shown to result in different blood volume patterns [19]. In the original work [20], the fingernail sensor contained a one-dimensional array of photodetectors and was capable of measuring only normal touching force. However, in this paper, a new fingernail sensor containing a two-dimensional array of photodetectors is used in order to detect and distinguish between normal forces, shear forces, and finger posture.

In previous work [20], a nonlinear dynamic model was created, based on physical laws and physiological knowledge, to relate normal force to photodiode outputs in a physically meaningful way. This physical model could in principle be extended to account for shear forces and bending in addition to normal force; however, the tissue mechanics are so complex that obtaining an accurate physical model for predicting bending and three axes of touch force is impractical.

Instead, the goal of this paper will be to develop a purely mathematical, data driven or “black box” model that can predict the fingertip force and posture as functions of the photodiode outputs. Both linear and nonlinear models will be considered and evaluated. A method is developed to uniformly calibrate the predictor to each user for all usable combinations of normal and shear forces. Calibration experiments are then performed to train and validate the predictor. Finally, performance of the predictor is analyzed and compared for the different models.

Manuscript received June 11, 2002; revised April 5, 2003. This work was supported in part by the National Science Foundation under Grant NSF IRI-0097700. This paper was presented in part at the IEEE International Conference on Robotics and Automation, Washington, DC, 2002. Experiments in this work received approval from the MIT Committee on the Use of Humans as Experimental Subjects.

The authors are with the d’Arbeloff Laboratory for Information Systems and Technology, Department of Mechanical Engineering, Massachusetts Institute of Technology, Cambridge, MA 02139 USA (e-mail: smascaro@mit.edu; asada@mit.edu).

II. PRINCIPLE AND EXPERIMENTAL APPARATUS

A. Fingernail Color Changes

When the human finger is flexed or pressed down against a surface, the blood volume under the fingernail changes and a variety of color patterns are visible through the fingernail. Fig. 1 shows the variables of interest that influence the coloration of the fingernail. These include the normal force, F_z , the lateral shear force, F_x , and the longitudinal shear force, F_y , which occur when the finger is pressed against a surface. Since the finger surface is curved, the direction of force and its influence on coloration vary, depending on the location, contact angle, and the shape of the contact surface. For this paper, we focus on the case where the fingerpad is pressed against a large, uniformly flat surface parallel to the bone of the distal phalanx, such that the contact area is maximized and the contact is most stable. Thus the contact location is irrelevant and the three touch force directions are defined with respect to the surface.

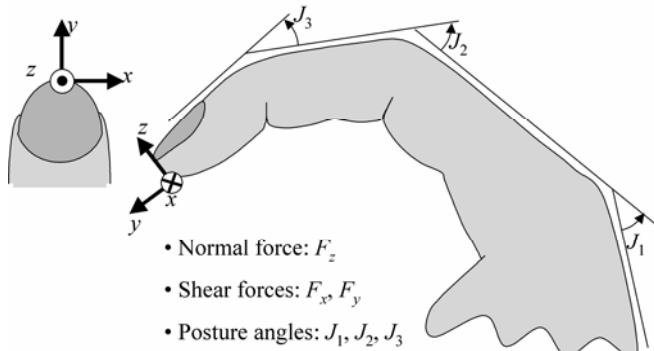


Fig. 1. Finger variables of interest. The forces are defined to be positive when the finger is pressed against a surface in the positive x , y , and z directions as shown. The finger posture is represented by the angle of the knuckle (MP) joint, J_1 , the middle (PIP) joint, J_2 , and the distal (DIP) joint, J_3 . The angles are defined to be positive for flexion and negative for extension (the finger can typically be hyper-extended to -10°).

Also of interest are the three posture angles, J_1 , J_2 , and J_3 . However in practice, J_1 does not affect the fingernail color; also J_3 is coupled to J_2 , as long as the finger is not in contact with the surface when bending occurs, an assumption that will be addressed later in Section III-A. Therefore in this paper, the only posture angle of interest is J_2 , hereafter referred to as θ .

Fig. 2 shows a typical set of fingernail colorations for a single human subject. The subject was directed to assume eight different force/posture poses by pressing down on a force sensor or bending the finger, while the fingernail was imaged from above using a digital CCD camera. Normal force, negative and positive lateral shear force, negative and positive longitudinal shear force, extension and flexion all result in visibly different patterns of coloration. In addition, the same general patterns of coloration occur for all people with healthy fingernails. Fig. 3 shows the average fingernail color patterns for 16 human subjects of various size, gender,

and skin color.

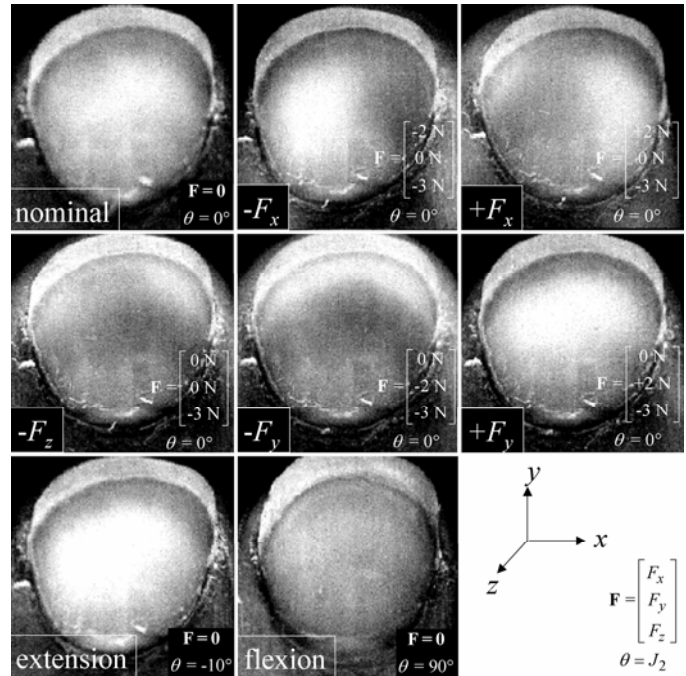


Fig. 2. Fingernail coloration for a single human subject. Eight different force/posture poses are shown. 5x contrast is applied.

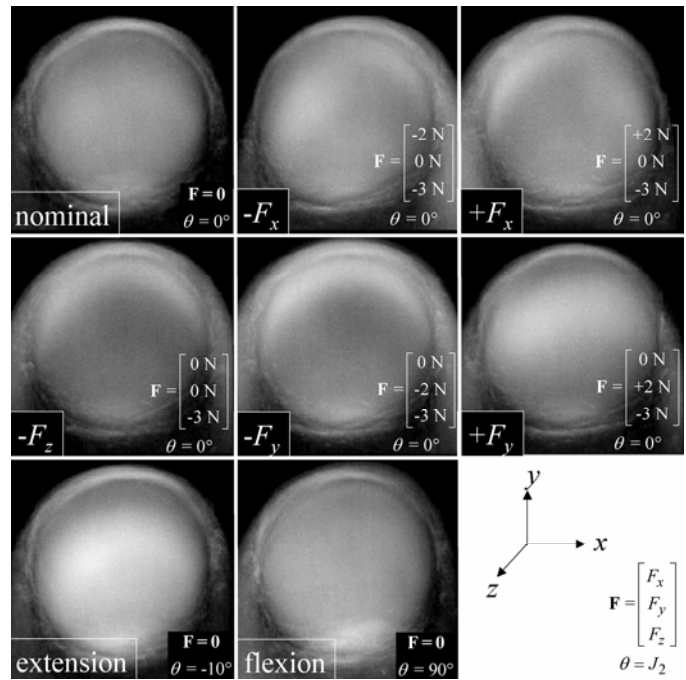


Fig. 3. Average fingernail coloration for 16 human subjects for the same eight poses. Images from the 16 subjects were normalized to the same size and averaged pixel by pixel. 5x contrast is applied. Subjects were instructed to apply the same constant forces using visual feedback from the force sensor.

The differences in the color patterns are further demonstrated in Fig. 4, where a threshold filter is used to highlight regions of white and dark, corresponding to regions of more and less blood, respectively.

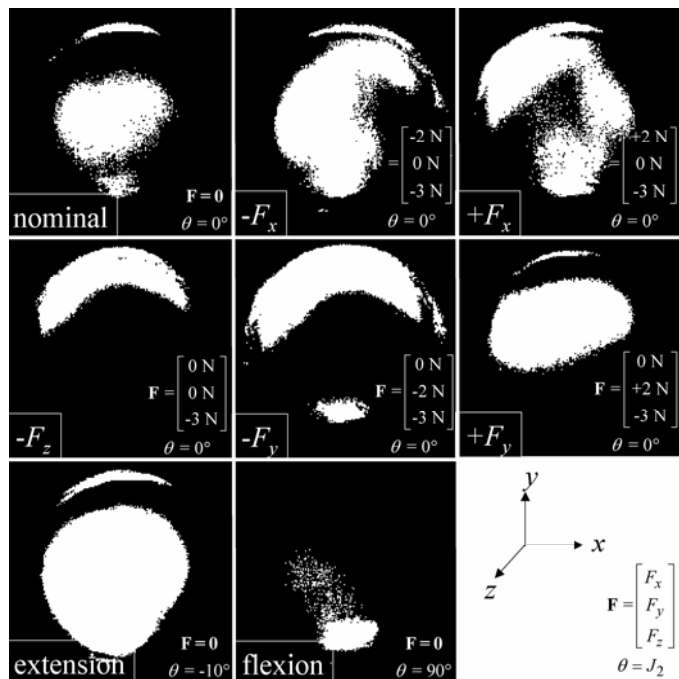


Fig. 4. Average fingernail coloration for 16 human subject with threshold filter applied for the same eight poses.

B. Fingernail Sensor

Based on the above experiments on fingernail coloration, we can develop an optical fingernail sensor. When light is emitted into the fingernail and the reflected light is measured by a photodiode, the photodiode output depends on the volume of blood, which is the principle of the fingernail sensor. Thus a fingernail sensor that measures these two-dimensional color patterns should be able to detect and distinguish between normal force, shear forces, and extension/flexion.

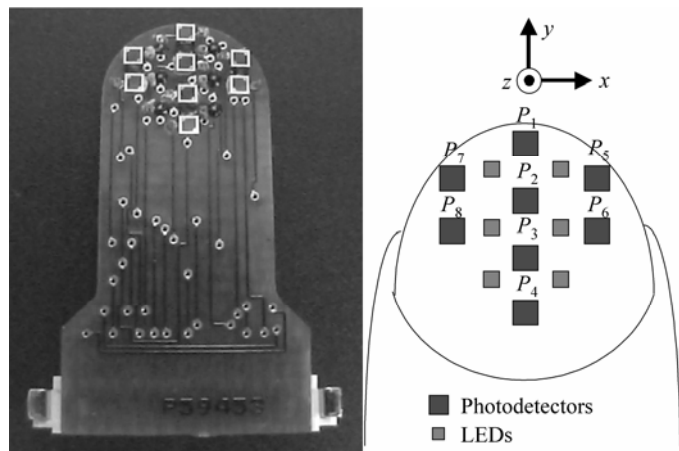


Fig. 5. Fingernail sensor with 2-D array of photodiodes. On the left is a partially assembled sensor. On the right is a schematic of the sensor array relative to the fingernail.

In this paper, an advanced fingernail sensor prototype with a two-dimensional array of photodiodes is used, as shown in Fig. 5. Six LEDs and eight photodiodes are placed on the fingernail surface to measure the blood volume at eight locations. The wavelength is chosen to be near the isobestic

point (~800nm), where the absorption is independent of blood oxygen levels. The closest commercially available LED chips emit at 770nm.

Fig. 6 shows a human subject wearing a fully assembled fingernail sensor and pressing against a calibration stand. The fingernail sensor has been molded to the shape of the fingernail and attached using a transparent adhesive tab. A three-axis force sensor is placed beneath the fingertip to measure the actual normal and shear forces during calibration. In order to measure the posture angles, a video tracking system is used to track the positions of colored markers placed along the finger.

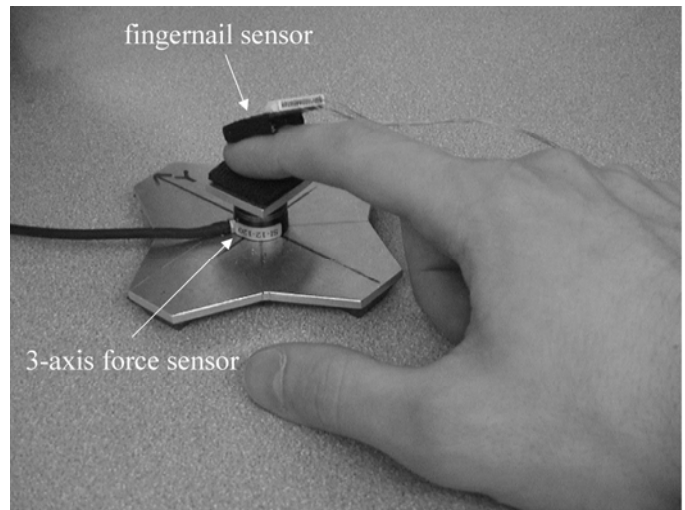


Fig. 6. Experimental apparatus for measuring touch force. A 3-axis force sensor underneath the fingertip measures actual normal and shear forces.

III. PREDICTOR DESIGN

A. Modeling Goals

Preliminary experiments show that the photodiodes do respond with different patterns of signals to changes in normal force, F_z , lateral shear force, F_x , longitudinal shear force, F_y , and change in finger posture, θ . The goal of this section is to design a multi-input, multi-output filter that receives the photodiode signals and inputs and predicts the three forces and bending angle. Since the model parameters will vary from user to user, the model will be calibrated by experimentally tuning the parameters for each user. To calibrate the model so that it can predict any combination of touch forces and bending angle, all four variables should be simultaneously varied in all possible combinations while the photodiode outputs are recorded. However, this leads to two major problems:

1. It is extremely difficult to simultaneously vary and measure the three forces and bending angle in a controlled manner.
2. When force is applied to the fingertip, the angles of the DIP and PIP joints are no longer coupled and can vary independently.

In this paper, we limit the functional requirements and applications to prediction of either touch or bending but not both simultaneously. In other words, the sensor is to measure

three axes of touch force while the finger is in contact with the environment, and measure the bending angle when the fingertip is free of contact.¹

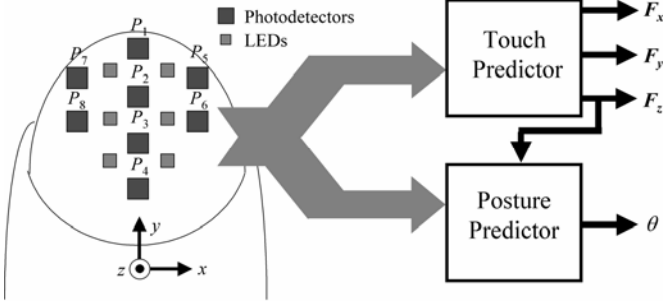


Fig. 7. Dual touch/posture predictor. Posture predictor turns on when normal touch force is below some threshold.

In this case, the predictor can be split into two separate predictors as shown in Fig. 7, one for force and one for bending, which can then be calibrated separately. If the force predictor is programmed to be resistant to bending (i.e. predict zero force in the presence of bending), then the posture predictor can simply be activated whenever the touch-force predictor predicts zero force.

The triple-output touch-force predictor must still be calibrated by simultaneously varying all three forces and thus is more complicated than the single-output posture predictor. Therefore this paper will focus on the design and calibration of the touch predictor. However the same types of models can be used for the bending predictor and calibration results will be presented for both. Three different types of regression models will now be proposed as candidates for the framework of the two predictors.

B. Linear Regression Model

The simplest model that can be used for the touch-force predictor is a linear regression model. Each variable of interest will be a linear combination of the outputs of the m photodiodes (for the current prototype, $m = 8$):

$$\hat{\mathbf{F}} = \begin{pmatrix} \hat{F}_x \\ \hat{F}_y \\ \hat{F}_z \end{pmatrix} = \mathbf{J}_F \mathbf{P} + \mathbf{F}_0, \quad (1)$$

where \mathbf{P} is an $m \times 1$ vector of photodetector outputs, $\hat{\mathbf{F}}$ is a 3×1 vector of force predictions, and \mathbf{J}_F is the $3 \times m$ experimentally determined matrix relating the two. \mathbf{F}_0 is the experimentally determined force offset vector. Equation (1) reduces to a homogeneous equation by augmenting vector \mathbf{P} and combining matrix \mathbf{J}_F and vector \mathbf{F}_0 together:

$$\hat{\mathbf{F}} = \tilde{\mathbf{J}}_F \tilde{\mathbf{P}}, \quad (2)$$

where $\tilde{\mathbf{J}}_F = [\mathbf{J}_F, \mathbf{F}_0]$ is a $3 \times (m+1)$ matrix and $\tilde{\mathbf{P}} = [\mathbf{P}^T, 1]$ is

an $(m+1) \times 1$ vector. To determine $\tilde{\mathbf{J}}_F$, a multivariate linear least squares regression is performed using n sets of experimental data.

Let \mathbf{Y} be a $3 \times n$ matrix consisting of the n sets of experimentally measured forces, F_x , F_y , and F_z , and \mathbf{B} be a $(m+1) \times n$ matrix containing the corresponding n sets of measured photodiode outputs. The optimal regression matrix $\tilde{\mathbf{J}}_F^*$ that minimizes the squared prediction errors is given by:

$$\tilde{\mathbf{J}}_F^* = \mathbf{Y} \mathbf{B}^T (\mathbf{B} \mathbf{B}^T)^{-1} \quad (3)$$

A similar regression model can be obtained for the bending predictor where the 3-D force vector is replaced by the 1-D posture angle.

C. Polynomial Model

In order to achieve a model that fits the data more closely, a nonlinear regression could be performed. Since preliminary \mathbf{P} vs. \mathbf{F} data shows some curvature, it is reasonable to try a polynomial model. The more terms in the polynomial, the better the model can fit the curvature. As a start, a second-degree polynomial model is considered, the most comprehensive of which includes all the squares and cross products of the photodetector readings:

$$\hat{\mathbf{F}} = \begin{pmatrix} \hat{F}_x \\ \hat{F}_y \\ \hat{F}_z \end{pmatrix} = \mathbf{J}_F \mathbf{P}_Q + \mathbf{F}_0, \quad (4)$$

where \mathbf{P}_Q is the vector $[P_1, P_2, \dots, P_m, P_1^2, P_1 P_2, P_1 P_3, \dots, P_1 P_m, P_2^2, P_2 P_3, \dots, P_2 P_m, \dots, P_m^2]^T$, the dimension of which is $M = m(m+3)/2$. $\tilde{\mathbf{J}}_F^*$ is computed as before using experimental training data, except that \mathbf{B} is now an $(M+1) \times n$ matrix containing n samples of the photodiode outputs.

D. Neural Network Model

Neural network models can also be used to approximate nonlinear functions [21]. A basic three-layer feedforward neural network model can be used to predict the three touch forces based on the m photodiode signals. Let the hidden layer consist of N nodes, each of which outputs a nonlinear function of a weighted and biased sum of the photodiode signals. The output layer then produces estimates of the three forces, each of which is the weighted and biased sum of the N outputs of the hidden layer. The total number of parameters involved in the three-layer neural net is $(m+4)N+3$.

Each neural network model is trained using a standard backpropagation algorithm on a set of training data. In order to avoid over-training, a set of validation data is used to halt training when the validation performance no longer improves. The optimal number of hidden nodes is experimentally determined by iteratively increasing N and retraining until the performance no longer improves.

¹ Note that since touching and bending are now exclusive actions, J_3 can indeed be treated as coupled to J_2 during bending, and can thus be eliminated as an independent variable.

IV. PREDICTOR CALIBRATION

A. Method

In order to calibrate the touch predictor using any of the three types of models (linear, polynomial, neural network), a set of training data is needed, consisting of readings from each of the m photodiodes and corresponding values of the three touch forces as measured by a three-axis force sensor placed beneath the finger.

In order to calibrate the force predictor to predict any possible combination of touch forces, the training data should be distributed across the entire usable portion of the three-dimensional force space. Therefore, a means is needed to prompt the user to fully explore this space during the training session. Since it is difficult for a human to apply desired forces simultaneously in three dimensions, the desired forces and the actual forces (measured by the experimental platform) should be visually presented to the user in an intuitive manner.

In the past, three-dimensional force information has been visually presented using a pseudo-perspective view with horizontal, vertical, and diagonal bars representing each of the forces [22]. However this requires the user to track three different positions on the screen at once. Instead, to achieve a more intuitive feedback, the information should be presented in such a way that the user must only track a single position on the screen.

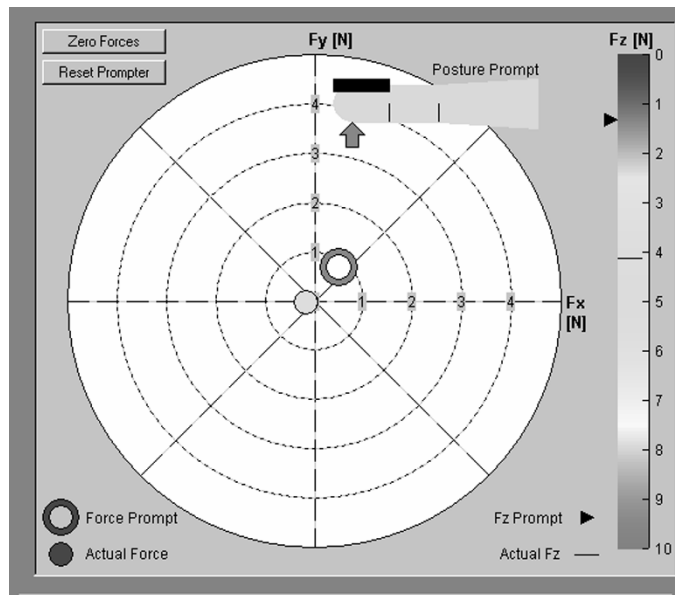


Fig. 8. Graphic user interface for calibration. The user tries to keep the circle within the moving ring while matching the color of the circle to that of the ring. The bar on the right also displays normal force, providing an alternative to matching the colors.

Fig. 8 shows a graphic user interface (GUI) that will be used as an intuitive force prompter. Two of the three dimensions of force are represented by position, while the third dimension is represented by color. The small circle in the center of the white display represents the actual force applied, as measured by a three-axis force-sensing platform placed beneath the finger. The ring represents the desired force generated by the prompter. The goal of the user is to keep the

circle within the ring and match the color at the same time, while the prompter moves the ring along a prescribed trajectory. The x -positions of the circle and ring represent lateral shear force F_x , the y -positions represent longitudinal shear force F_y , and the colors represent normal force F_z . The

bar on the right side of the GUI provides an alternate, redundant display of normal force. It is not critical that the actual forces are identical to the prompted forces. The actual forces, measured by the force sensor, are used for training the predictor. The prompts are only a guide to fully exploring the force space.

In the previous section, it was mentioned that the touch predictor must also be trained to predict zero force in the presence of bending. Therefore, the GUI in Fig. 8 also includes a posture prompt in the form of a graphically illustrated finger. Before the touch prompting begins, the user is prompted to bend the finger in synchronization with the finger on the screen, while readings of zero force are registered. The training data for the force predictor then contains a number of samples with zero force, whose photodiode readings correspond to finger bending. The posture prompt is also used to generate training data for the posture predictor during a separate posture calibration session. The actual posture is measured using a video tracking system where colored markers are placed along the length of the finger.

B. Constraints

(1) *Range of Calibration:* The usable portion of the force space is constrained by three factors:

1. The range of forces that a human can comfortably apply and control.
2. The range of sensitivity of the fingernail sensor.
3. The coefficient of friction of the finger against the surface of contact.

A number of references discuss the capability of the human to apply normal forces with the fingertip. As reported in [6], normal forces in the range of 0 to 2 N are most relevant for examining the response of the fingerpad during grasping and typing. According to [23], a human is capable of controlling a constant force in the range of 2 to 6 N with average error of 6% using visual feedback in addition to natural haptic sense. However, when shear force is added, the maximum normal force that a human subject can comfortably apply for an extended time (i.e. a few minutes) is about 3 N. Preliminary experiments conducted indicate that this is within the range of sensitivity of the fingernail sensor.

The ability of the human to apply shear forces depends on the coefficient of friction between the finger skin and the surface of contact. To maximize the shear force during calibration, the experimental platform is covered with a soft rubber material, with an experimentally determined static coefficient of friction of approximately 0.75. Therefore, if the normal force ranges between 0 and 3 N, the total shear force can range between 0 and 2.25 N. Preliminary experiments indicate that this also is within the range of sensitivity of the

fingernail sensor.

(2) *Speed of Calibration*: To make calibration as convenient as possible, the total training time should be minimized. However, the speed of calibration is also constrained by the dynamics of the fingertip system. If the user is prompted to explore the force space too quickly, the sensor response will lag too much behind the applied force due to viscoelastic dynamics.

If the fingertip dynamics are approximated as a linear system dominated by its slowest time constant, τ_{\max} , and the force is changing at a rate \dot{F} , then the steady-state lag in photodiode output is given by $\Delta P = \dot{P} \tau_{\max}$.

If this apparent error in photodiode output is expressed as a percentage, then

$$\% \text{ error} = \frac{\Delta P}{P} = \frac{\dot{P} \tau_{\max}}{P} \approx \frac{\dot{F} \tau_{\max}}{F} = f \tau_{\max}, \quad (5)$$

where $f = \dot{F}/F$ is the percent rate of change of force. Therefore, if the time constant is known and a limit is set on the allowable percent error, the maximum f can be calculated and used as a constraint on the speed of the prompter.

The experiments in [20] indicate that the effective time constant of the sensor response is between 0.1 and 0.4 seconds. This is comparable to the viscoelastic time constants of the fingerpad determined by [6]. Therefore, if the %error in (5) is constrained to be 10%, and $\tau_{\max} = 0.1$ s, then the maximum allowable rate of change of force, f_{\max} , is 100% per second, which is 1 s^{-1} or 1 N/s per N . Based on the results in Section V, the choice of 10% error here is not likely to be the limiting factor on predictor performance.

C. Trajectory Design

The next task is to design the calibration trajectory that the force prompter will execute in order to lead the user to explore the entire force space while a set of training data is collected. The force space to be explored consists of a three dimensional cone defined by the constraints of maximum normal force and frictional shear force, as depicted in Fig. 9.

To efficiently explore this cone-shaped space, an upward moving, spiraling and circling trajectory can be designed as shown in Fig. 10. As the normal force gradually increases from zero, the magnitude of shear force periodically increases and decreases while the direction of the shear force circles around. Due to the frictional constraint, the range of possible shear force magnitudes increases linearly with normal force. However the training data should be spread uniformly across the cone-space in order to create a predictor that is not biased toward any specific portion of the space (unless a specific application suggests otherwise).

The training data can be specified to be of uniform density in either cylindrical coordinates or Cartesian coordinates. If cylindrical coordinates are chosen, the predictor will be unbiased in terms of magnitude and direction of shear force; whereas if Cartesian coordinates are chosen, the predictor will

be unbiased in terms of the magnitudes of the individual shear force components. Which method is chosen depends on the application of the predictor. In either case, the training data should be uniform in magnitude of normal force.

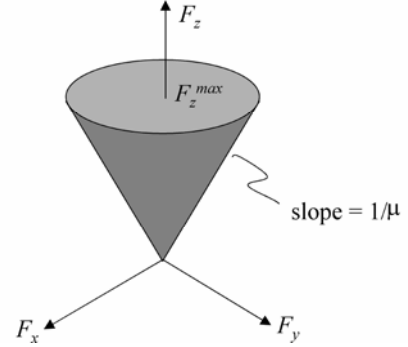


Fig. 9. 3-D force space. Possible combinations of normal and shear forces form a cone.

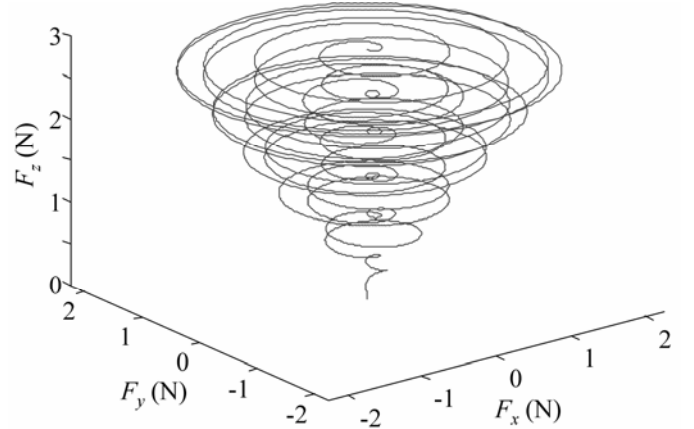


Fig. 10. 3-D calibration trajectory. Normal force slowly increases while shear force oscillates in magnitude and circles in direction.

In order to create a set of training data with a uniform cylindrical density, the time spent to explore the range of shear force needs to increase linearly with normal force. This relationship can be expressed in differential form relating infinitesimal time interval to infinitesimal change in normal force F_z :

$$dt = \alpha F_z dF_z, \quad t = T \Rightarrow F_z = F_z^{\max}. \quad (6)$$

Solving (6) with the boundary condition that the maximum normal force is reached at time T gives a formula for normal force as a function of the square root of time:

$$F_z = F_z^{\max} \sqrt{t/T}, \quad F_z^{\max} = 3 \text{ N}, \quad (7)$$

where F_z^{\max} is given as shown by the range constraint, and T will be determined later from the speed constraint.

Next, in order to create the spiraling action, the magnitude of the shear force, F_r , should oscillate between the minimum and maximum possible values, $\pm \mu F_z$. If F_r is given by

$$F_r = \mu F_z \sin(2\pi f_s F_z), \quad \mu = 0.75, \quad f_s = 1.0 \text{ N}^{-1}, \quad (8)$$

then F_r oscillates smoothly between the limits in an approximately uniform manner. A value of $f_s = 1.0 \text{ N}^{-1}$

creates one cycle of radial oscillation per unit of normal force. The maximum radial velocity is

$$\text{Max}\left(\frac{dF_r}{dt}\right) = \frac{\mu\pi f_s (F_z^{\max})^2}{T} \quad (9)$$

and will be used with the speed constraint to choose T .

Finally, in order to create the circling action, the direction of the shear force should rotate around with constant speed. The lateral and longitudinal components of the shear force are thus given by

$$F_x = F_r \sin(2\pi f_c t), \quad F_y = F_r \cos(2\pi f_c t), \quad (10)$$

where f_c is the circling frequency. The ratio of the circling frequency to the radial velocity determines how many times the trajectory circles around for each unit of radial motion. To uniformly cover the force space, the circling frequency should be high enough to complete one or two circles per unit of radial motion. Assuming the circling action takes place much faster than the radial motion and the z -motion, the percent rate of change of force is approximately $2\pi f_c$. The speed constraint f_{\max} from Section IV-B2 can then be used to choose f_c :

$$2\pi f_c < f_{\max} \Rightarrow f_c < \frac{1\text{s}^{-1}}{2\pi} \Rightarrow f_c = 0.15 \text{ Hz} \quad (11)$$

This then places a constraint on the maximum radial velocity from (9). To ensure the time to complete one circle is less than the time to move one radial unit, the following equation must be satisfied:

$$\frac{1}{f_c} < \frac{T}{\mu\pi f_s (F_z^{\max})^2} \Rightarrow T > 140\text{s}. \quad (12)$$

Thus, by choosing a total calibration time $T = 180\text{s}$ (3 min), the trajectory will complete slightly more than one circle per radial unit. This is small enough that calibration is not overly fatiguing or impractical. Putting everything together, the 3-D trajectory of Fig. 10 is achieved.

A similar trajectory could be derived in order to achieve training data with a uniform Cartesian density.

V. EXPERIMENTS AND ANALYSIS

A. Touch Prediction

Using the calibration method detailed in Section III, touch-force predictors were trained for seven different human subjects. Each subject practiced following the force prompt and then executed the training routine three times.² The first two times, the data was collected and used to train the predictor using the linear, polynomial and neural network models. The third time, the data was collected and used to validate the performance of the predictors (and to halt the backpropagation in the case of the neural network model).

² Results show that the predictor performs significantly better on test data if calibrated using two sets of training data. This could be due to unmodeled variations between training sessions, such as slight variations in the posture of the finger relative to the force-sensing platform. When two sets of data are used for training, it forces the model to train to the features that remain constant between training sessions.

Each time, the subject was first prompted to bend the finger back and forth a few times. Then the subject was instructed to extend the finger to $\theta = 0^\circ$ and place the fingerpad flat down against the surface of the force-sensing platform, and then follow the trajectory of the force prompt. Finally, each subject was requested to execute a fourth routine with a random force trajectory to use as a final test of predictor performance.

Fig. 11 shows sample training data from a single subject with the force predictions of the linear model plotted overtop. In this case, the predictions are simply a measure of how well the model fits the training data. The actual forces are zero for the first 60 seconds as the finger is bent back and forth. Then the normal force slowly increases in the negative direction while the two shear forces oscillate with increasing magnitude.

Fig. 12 shows sample validation data from the same subject. Data from a third spiral trajectory is followed and the forces are predicted based on a linear model that was trained on the first two spirals. The force predictions are plotted overtop of the actual measured forces. In this case, there is a slight degradation in the predictor performance, but the predictor still performs well.

Finally, Fig. 13 shows sample test data using a random trajectory. In this case the subject began with 20 seconds of bending followed by 100 seconds of random motion through the force space. The same predictor that was calibrated using the first two spirals was then used to predict the forces for the test data. In this case, the predictor performs well for the shear forces, but performs significantly worse for the normal force.

Figs. 14-16 compare the average performances (over all seven subjects) of the three types of models for training, validation and testing. As shown in Fig. 14, the polynomial model fits the training data with the least error due to the large number of parameters. However, as shown in Fig. 15, the polynomial model has the worst error when predicting the forces for the test data, especially the normal force, F_z . While the polynomial model is better able to fit the curvature of the data, it actually over-trains itself to the noise in the training data and cannot generalize to predict forces for new data.

The linear and neural network models both show comparable performance for fitting the training data and predicting all three forces for the validation data. The neural network has more flexibility to fit the data, but is prevented from over-training by the validation check. To further examine the linear and neural network models, performances can be compared for the random test data. When presented with new random data, the linear model performs better on average than the neural network model for all three forces. Especially for the two shear forces, the linear model has a consistently lower RMS error in predicting new random data. Therefore, the linear model, which also has the advantage of being less complex and faster to train, should be used. Using the linear model, the two shear forces are predicted with average RMS errors of 0.4 to 0.5 N, while the normal force is predicted with an average RMS error of 1.0 N.

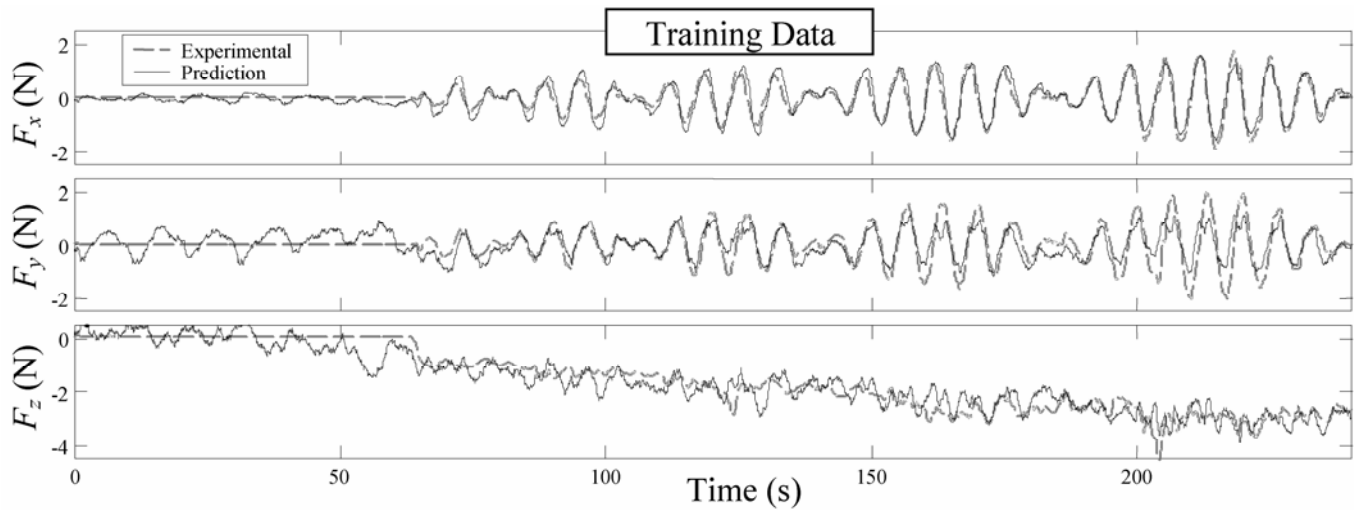


Fig. 11. Sample training data for touch predictor for a single subject. Data belongs to one of two consecutive spiraling trajectories used to train the model. Predicted forces using the linear model are superimposed on experimental forces measured by 3-axis force sensor.

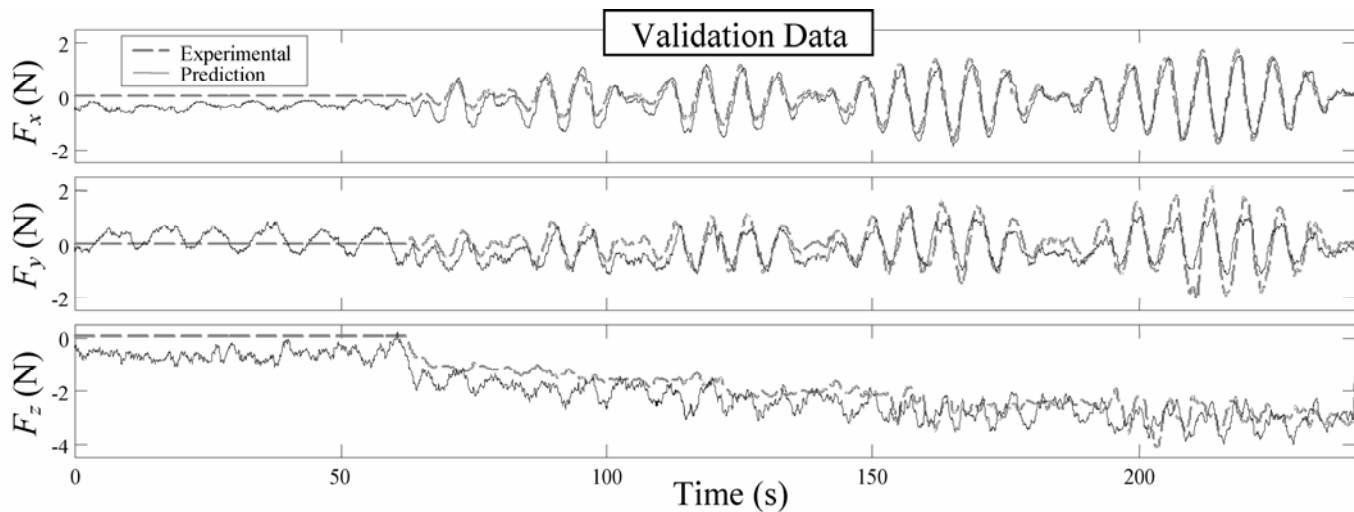


Fig. 12. Sample validation data for touch predictor for a single subject. Data belongs to third spiraling trajectory that is used to validate the model. Predicted forces using the linear model are superimposed on experimental data.

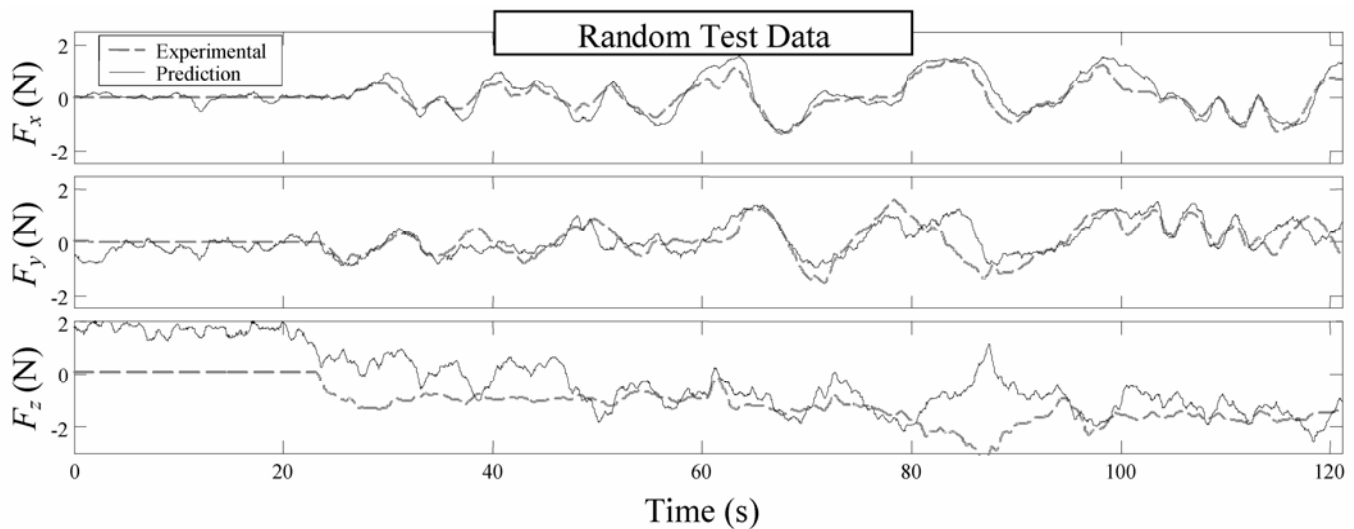


Fig. 13. Sample test data for touch predictor for a single subject. Data belongs to a random user-generated trajectory that is used to test the model. Linear model predictions are again superimposed.

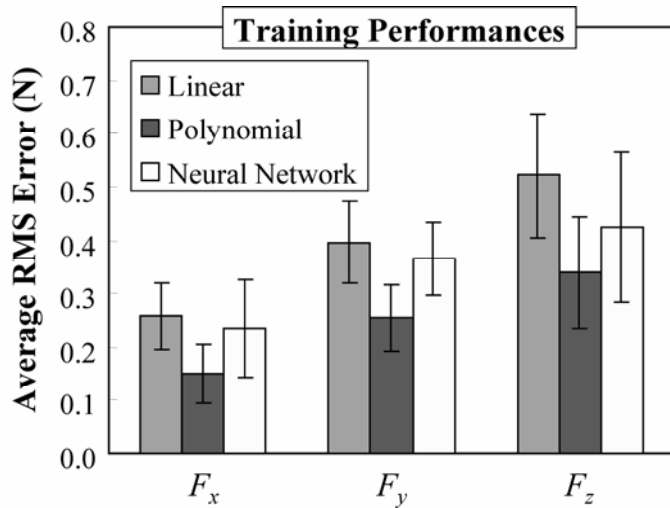


Fig. 14. Training performance for touch predictor. RMS errors of model predictions are averaged for 7 human subjects. The polynomial model fits the training data with the least error.

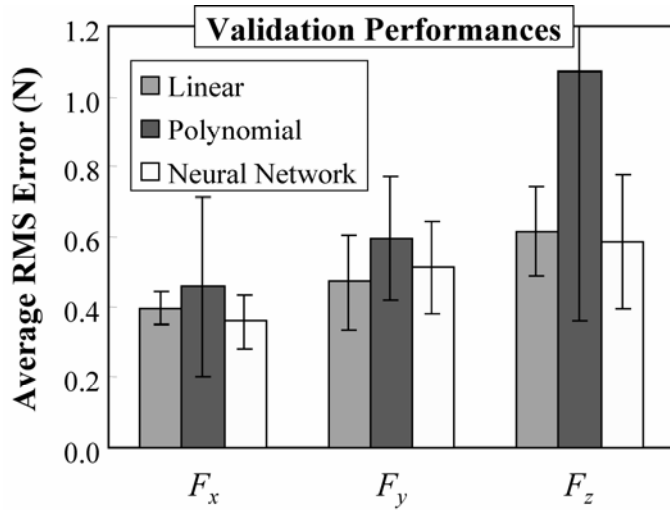


Fig. 15. Validation performance for touch predictor for same 7 subjects. The polynomial model performs the worst when presented with new validation data.

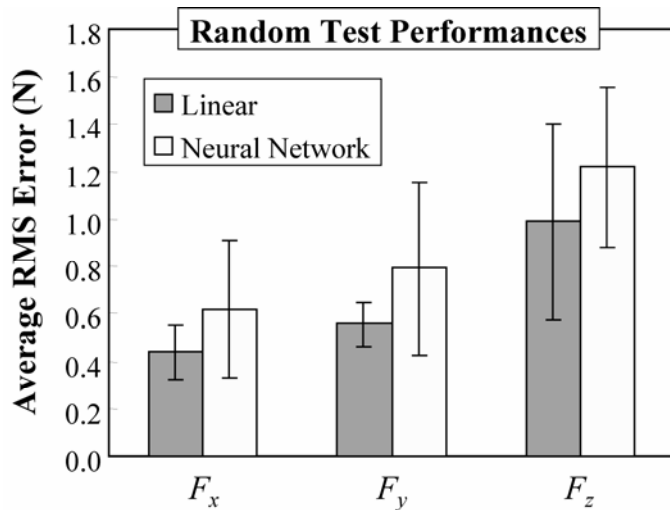


Fig. 16. Test performance for touch predictor for same 7 subjects. The linear model performs better than the neural network model when presented with new random test data.

When comparing the random test performances with the validation performances, it is important to note that the errors in predicting the shear forces are almost identical, while the error in predicting normal force is significantly larger for the random case. This indicates that while the spiraling trajectory may be very good for calibrating the shear forces, it is not a good trajectory for calibrating normal force. The obvious difference is that the normal force, unlike the shear forces, is not oscillating at all. In future experiments, the effect of building some normal force oscillation into the calibration trajectory should be investigated as a means for improving performance.

B. Posture Prediction

Bending experiments were also performed using the same seven subjects. Each subject was instructed to slowly flex and extend the finger for six cycles at a rate of 0.1 Hz, following the posture prompt in the GUI. Fig. 17 and Fig. 18 show sample training and validation data for a typical subject using a linear model.

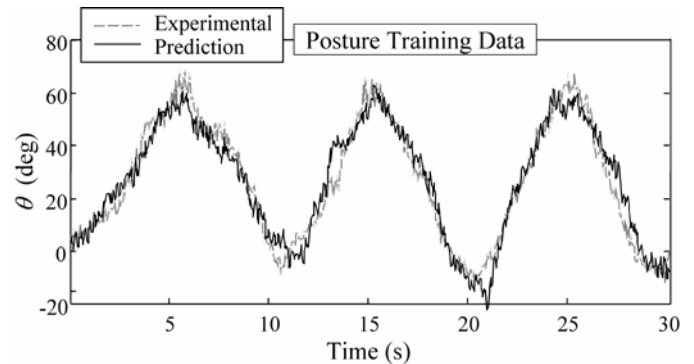


Fig. 17. Training data for posture predictor for a single subject. Model is trained using first half of 60 second data set. Predicted posture angle for the linear model is superimposed on the experimental posture measured by the video tracking system.

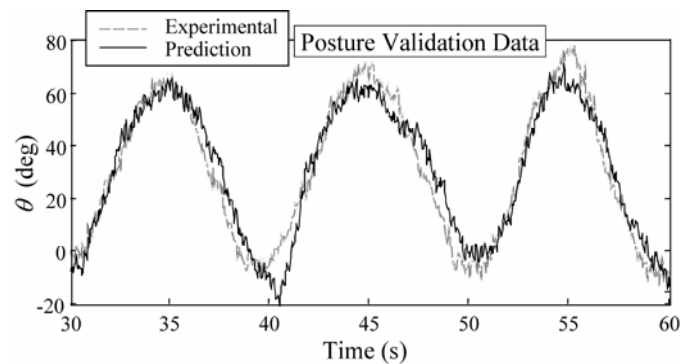


Fig. 18. Validation data for posture predictor for a single subject. Model is validated using second half of data set. Predicted posture angle for the linear model is superimposed on experimental data.

The performance of the posture predictor should also be compared for the three types of models. Fig. 19 shows the average training and validation performances for the three models when predicting the angle of the PIP joint. As with the touching, the polynomial model over-trains to the data and cannot generalize to the validation data. Looking at the validation performances, the polynomial model should again

be ruled out, while the neural network and linear models both perform comparably. The neural network does perform slightly better, predicting the bending angle with an average RMS error of 8 degrees, compared to 10 degrees for the linear model. In this case, either the linear or neural network model could be chosen, depending on the relative importance of simplicity vs. performance.

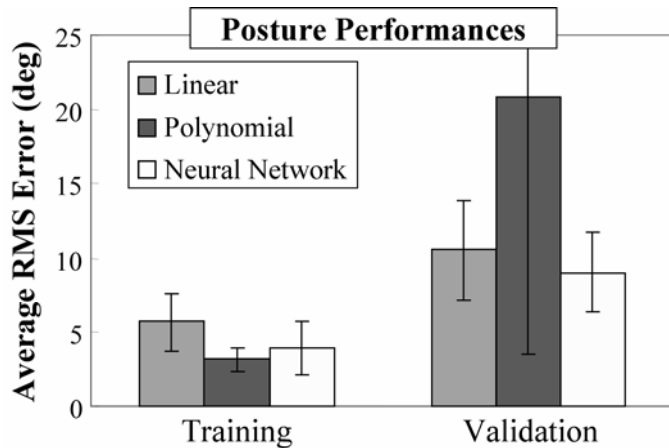


Fig. 19. Performance of posture predictor for training and validation. RMS errors of model predictions are averaged for 7 human subjects. Polynomial model fits training data better but again performs worst when presented with new validation data. Linear and neural network models are again comparable.

VI. CONCLUSIONS

In conclusion, a new fingernail sensor with a two-dimensional array of photodetectors has been created in order to measure the two-dimensional color patterns of the fingernail that results from changes in finger posture and application of three-axes of touch forces.

A multi-input, multi-output predictor has been designed to predict normal and shear forces at the human fingertip as well as posture angle based on the photodiode readings from the fingernail sensor. An intuitive GUI was created to calibrate the predictor for each user for all possible combinations of normal and shear forces. Despite variations in user sensitivity and haptic coordination, the predictor was successfully calibrated for seven different human subjects. Experiments show that a linear model performs best in predicting random combinations of touch forces, predicting shear force with average RMS errors of 0.5 N and normal force with an average RMS error of 1 N. For the posture predictor, linear and neural network models perform comparably well, both predicting posture angle with an average RMS error of 10 degrees or less.

The average RMS errors in the shear forces are approximately 10% of the shear force range (-2.25 N to +2.25 N), which would at least be sufficient for providing some input to a computer or robot. The average RMS error of the posture predictor is also 10% of its range (-10° to 90°), making it equally useful. However, the large average RMS error of 1 N for normal force is unsatisfactory, especially since the range of normal forces is only 0 to 3 N. In future experiments, the calibration trajectory will be redesigned to include oscillation in normal force as well as shear force in an

effort to improve this performance. In the meantime, the utility of the sensors may be best suited for applications such as an alternative computer mouse, where the shear forces are used to control the 2-D velocity of the cursor on the screen, or finger bending is used for 1-D scrolling. Further analysis will also lead to more intelligent configurations of the LEDs and photodiodes that could improve predictor performance for all four variables of interest, allowing the sensor to be more useful for monitoring grasping and manipulation.

Performance can also be improved by shaping the sensor to the fingernail of each user to ensure proper adhesion of the sensor to the fingernail. In our experiments, human subjects having similar fingernail curvatures were selected for testing so they could all use the same sensor. In addition, the sensors were used in an indoor environment of constant temperature and the hand was kept at a constant elevation of desk level. In general, the performance of the predictors may be affected by variability in blood flow/pressure due to changes in finger temperature, hand elevation, or any other factors affecting cardiovascular activity. Further study is required in order to quantify the effects of any such variations.

REFERENCES

- [1] J. Webster, Ed., *Tactile Sensors for Robotics and Medicine*. New York: Wiley, 1988.
- [2] D. J. Sturman and D. Zeltzer, "A Survey of Glove-based Input," *IEEE Comp. Graph. Appl.*, vol. 14, no. 1, pp. 30-39, 1994.
- [3] N. Nakazawa, Y. Uekita, H. Inooka, and R. Ikeuri, "Experimental Study on Human's Grasping Force," in *Proc. IEEE Int. Workshop Robot Human Communication*, pp. 280-285, 1996.
- [4] S. Shimizu, M. Shimojo, S. Sato, Y. Seki, A. Takahashi, Y. Inukai, and M. Yoshioka, "The Relation between Human Grip Types and Force Distribution Pattern in Grasping," in *Proc. IEEE Int. Workshop Robot Human Communication*, pp. 286-291, 1996.
- [5] W.J. Peine and R.D. Howe, "Finger Pad Shape in Lump Detection," in *Proc. ASME Bioengineering Conf.*, BED-vol. 35, pp. 593-594, 1997.
- [6] D.T.V. Pawluk and R.D. Howe, "Dynamic Lumped Element Response of the Human Fingerpad," *J. Biomech. Eng.*, vol. 121, pp. 178-183, 1999.
- [7] D.T.V. Pawluk and R.D. Howe, "Dynamic Contact of the Human Fingerpad Against a Flat Surface," *J. Biomech. Eng.*, vol. 121, pp. 605-611, 1999.
- [8] E.R. Serina, C.D. Mote, Jr., and D. Rempel, "Force Response of the Fingertip Pulp to Repeated Compression-Effects of Loading Rate, Loading Angle and Anthropometry," *J. Biomech.*, vol. 30, no. 10, pp. 1035-1040, 1997.
- [9] R.J. Gulati and M.A. Srinivasan, "Human Fingerpad Under Indentation I: Static and Dynamic Force Response," in *Proc. ASME Bioengineering Conf.*, BED-vol. 29, pp. 261-262, 1995.
- [10] U. Singh and R.S. Fearing, "Tactile After-Images from Static Contact," in *Proc. ASME Dynamic Systems and Control Division*, vol. 64, pp. 163-170, 1998.
- [11] I. Kim and H. Inooka, "Determination of Grasp Forces for Robot Hands Based on Human Capabilities," *Contr. Eng. Practice*, vol. 2, no. 3, pp. 415-420, 1994.
- [12] M. Castro and A. Cliquet, Jr., "A Low-Cost Instrumented Glove for Monitoring Forces During Object Manipulation," *IEEE Trans. Rehab. Eng.*, vol. 5, no. 2, pp. 140-147, 1997.
- [13] H. Yun, D. Cannon, A. Freivalds, and G. Thomas, "An Instrumented Glove for Grasp Specification in Virtual-Reality-Based Point-and-Direct Telerobotics," *IEEE Trans. Syst. Man, Cybern. B*, vol. 27, no. 5, pp. 835-846, 1997.
- [14] K. Nagata, Y. Oosaki, M. Kakikura, and H. Tsukune, "Delivery by Hand between Human and Robot Based on Fingertip Force-Torque Information," in *Proc. IEEE/RSJ Int. Conf. Intelligent Robots and Systems*, pp. 750-757, 1998.

- [15] S. Mascaro and H. Asada, "Hand-in-Glove Human-Machine Interface and Interactive Control: Task Process Modeling Using Petri Nets," in *Proc. IEEE Int. Conf. Robotics and Automation*, Vol. 2, pp. 1289-1295, 1998.
- [16] R.D. Howe, and M.R. Cutkosky, "Sensing Skin Acceleration for Slip and Texture Perception," in *Proc. IEEE Int. Conf. Robotics and Automation*, pp. 145-150, 1989.
- [17] F. Zee, E.G.M. Holweg, W. Jongkind, and G. Honderd "Shear Force Measurement using a Rubber Based Tactile Matrix Sensor," in *Proc. IEEE Int. Conf. Advanced Robotics*, pp. 733-738, 1997.
- [18] H.-Y. Han, A. Shimada, and S. Kawamura, "Analysis of Friction on Human Fingers and Design of Artificial Fingers," in *Proc. IEEE Int. Conf. Robotics and Automation*, pp. 3061-3066, 1996.
- [19] S. Mascaro and H.H. Asada, "Finger Posture and Shear Force Measurement using Fingernail Sensors: Initial Experimentation," in *Proc. IEEE Int. Conf. Robotics and Automation*, pp. 1857-1862, 2001.
- [20] S. Mascaro and H.H. Asada, "Photoplethysmograph Fingernail Sensors for Measuring Finger Forces without Haptic Obstruction," *IEEE Trans. Robot. Automat.*, vol. 17, no. 5, pp. 698-708, 2001.
- [21] S.S. Haykin, *Neural Networks: A Comprehensive Foundation*. Upper Saddle River, NJ: Prentice Hall, 1999.
- [22] Sheridan, T. *Telerobotics, Automation, and Human Supervisory Control*. Cambridge, MA: MIT Press, 1992.
- [23] L. Jones, "Perception and Control of Finger Forces," in *Proc. ASME Dynamic Systems and Control Division*, vol. 64, pp. 133-137, 1998.



Stephen A. Mascaro (S'96-A'02) received the B.A. degree in physics from Houghton College, Houghton, NY, and the B.S. degree in mechanical engineering from Clarkson University, Potsdam, NY, both in 1995. He received the M.S. and Ph.D. degrees in mechanical engineering from the Massachusetts Institute of Technology (MIT), Cambridge, MA, in 1997 and 2002, respectively.

He is currently a Postdoctoral Associate in the Department of Mechanical Engineering at MIT,

working in the d'Arbeloff Laboratory for Information Systems and Technology. His current research interests include robotics and control, system dynamics, human-machine interaction, haptics, biomechanical and physiological modeling, and wearable sensors.

Dr. Mascaro received the Best Paper Award at the 1999 IEEE International Conference on Robotics and Automation for his original work on fingernail sensors. He is also a member of the American Society of Mechanical Engineers.



H. Harry Asada (A'85) received the B.S. in mechanical engineering from Kyoto University in 1973, and the M.S. and Ph.D. in Precision Engineering also from Kyoto University in 1975 and 1978, respectively.

He was a Research Scientist at the Robotics Institute of Carnegie-Mellon University prior to joining MIT as faculty in 1982. From 1985 to 1988 he held a faculty position in the Department of Applied Mathematics and Physics at Kyoto University. Since

1990 he has been a full professor in the Department of Mechanical Engineering at MIT. He specializes in robotics and control and also has broad research interests in biomedical engineering, system dynamics, engineering design, manufacturing, and communication systems.

Prof. Asada received the O. Hugo Shuck Best Paper Award in 1984 from the American Control Council, three Best Paper Awards at the IEEE Robotics and Automation Conference in 93, 97, and 99, and five Best Journal Papers from Journals of Advanced Robotics, Instrument and Control Engineering, and Systems and Control. He is the recipient of the 1998 ASME Dynamic Systems and Control Outstanding Researcher Award, and a Fellow of ASME.